Analysis for Typical Fault of 12.5 kV Cabinet Bushing Based on Electro-Thermal Coupling Simulation

Xuanhe Cao, Shan Li, Jianqing Yang, Yanyan Lu, Zhiwen Zhou, Jinlong Guo, Xing Li, and Chuyan Zhang

Abstract The cases of transformer outlet short circuit caused by the failure of cabinet bushing in the GIS are relatively common in the operation of the power grid. This article establishes an electro-thermal coupling finite element analysis model for the 12.5 kV cabinet bushing fault event of the No.1 main transformer in a 220 kV substation. The electric field distribution and temperature characteristics of the bushing about the fault are obtained by simulating the air gap defect inside the bushing, and the combination of the FEM and Townsend discharge Theory. And it was found that the partial discharge in the internal air gap of the bushing gradually caused the insulation degradation. The temperature rise effect of the bushing under the influence of short-circuit current further accelerates the occurrence of the faults.

Keywords Cabinet bushing · Insulation degradation · Breakdown · Electro-thermal coupling simulation

1 Introduction

The cabinet bushing is a key equipment in the Gas Insulated Switchgear (GIS) which bears the insulation of the busbar to the cabinet body, and its operational reliability affects the lifetime of the 10 kV systems [1, 2]. At present, dry bushing made of epoxy resin is widely used in substations, which has a compact structure and is maintenance free [3–6]. However, the high potential shielding suspension can cause air insulation breakdown between the busbar and the bushing. And the air gap defects

X. Cao · X. Li · C. Zhang (✉)
School of Information Engineering, China University of Geosciences, Beijing 100083, China
e-mail: zcy@cugb.edu.cn

S. Li
State Grid Xinjiang Electric Power Research Institute, Xinjiang, Urumqi 830011, China

J. Yang · Y. Lu · Z. Zhou · J. Guo
State Grid Xinjiang Integrated Energy Service Company Limited, Xinjiang, Urumqi 830011, China

X. Dong and L. Cai (eds.), *The Proceedings of 2023 4th International Symposium on Insulation and Discharge Computation for Power Equipment (IDCOMPU2023)*, Lecture Notes in Electrical Engineering 1102, https://doi.org/10.1007/978-981-99-7405-4_55

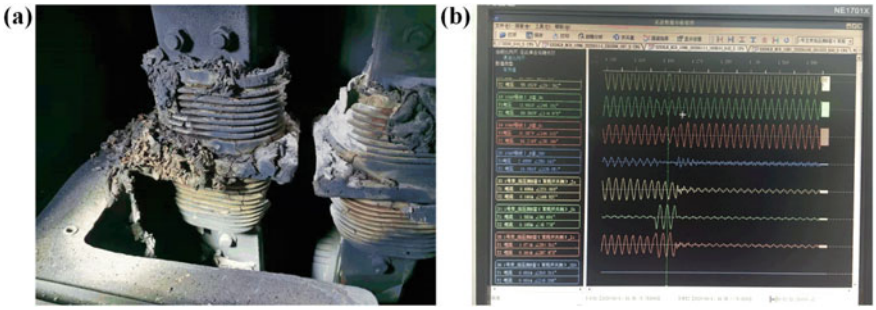

Fig. 1 **a** The accident site. **b** The fault waveform

present during the manufacturing process can also induce partial discharge, gradually leading to the aging of the insulation materials [7–10].

At present, there are many scholars researching on the calculation of the electric field and temperature field for the cabinet bushing under different voltage levels, which has a great reference value. However, there is a lack of physical field analysis of bushing under defect conditions in existing literature. And the connection of FEM simulation with the on-site operational accidents is weak.

This article conducts an electro-thermal coupling simulation and partial discharge analysis on a short circuit explosion accident of a 220 kV substation in Xinjiang, China, which occurred in January 2020. The analysis of the on-site accident data indicates that this event was caused by a three-phase short circuit fault on the low-voltage side of the No.1 main transformer. During the fault, the steady-state short-circuit current was 19.6 kA, with a duration of 1.69 s. The accident site and fault waveform are shown in Fig. 1.

2 The Finite Element Model

Based on the design drawings and material parameters of the bushing, an equal scale 3D simulation model of the 12.5 kV cabinet bushing was established in COMSOL Multiphysics. The model includes the bushing, busbar, installation flange, cabinet shell, and air domain. The bushing is mainly made of epoxy resin as the insulation material, and the model's geometry is shown in Fig. 2a. To simulate the degradation of the insulation of the bushing, randomly distributed internal air gaps were added for comparison, as shown in Fig. 2b.

The electric field distribution and the temperature distribution under the electrothermal coupling of the bushing are calculated respectively by using the three interfaces of COMSOL: Static electricity, Magnetic field and Solid and fluid heat transfer. The electric field control equation based on Poisson's equation is:

$$E = -\nabla V \tag{1}$$

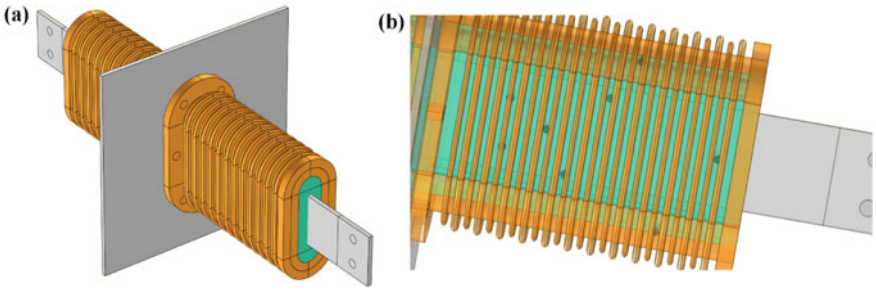

Fig. 2 **a** Simulation model of the cabinet bushing. **b** Internal air gaps of bushing

$$\nabla \cdot (\varepsilon_0 \varepsilon_r E) = \rho_v \tag{2}$$

where E is the electric field strength, V is the electric potential, ε_0 is the dielectric constant of vacuum, ε_r is the relative dielectric constant of the material, ρ_v is Volume charge density.

A partial differential equation system is built for electromagnetic thermal coupling to define and solve the heat transfer problem inside the bushing, where the magnetic field control equation is:

$$E = -j\omega A \tag{3}$$

$$\nabla \times H = J \tag{4}$$

$$\mu_0 \mu_r H = B = \nabla \times A \tag{5}$$

$$J = \sigma E + j\omega(\varepsilon_0 \varepsilon_r E) \tag{6}$$

The control equation that describing the heat transfer problem between solid and fluid inside the bushing is:

$$\rho C_p \frac{\partial T}{\partial t} - \nabla \cdot (k \nabla T) = Q_e = J \cdot E \tag{7}$$

$$-n \cdot q = h(T_{amb} - T) + \varepsilon\sigma(T_{amb}^4 - T^4) \tag{8}$$

where ρ is the density of the material; C_p is the heat capacity at constant pressure; T is the temperature; k is the thermal conductivity of the material; h is the Heat transfer coefficient of air convection. In Eq. (8), ε is the surface radiation coefficient; σ is the Stefan Boltzmann constant; T_{amb} is the external ambient temperature. In Eq. (7), the Fourier heat transfer term is used to describe the internal heat transfer of the bushing.

Table 1 The material parameters of the cabinet bushing

Material	Conductivity (S m)	Thermal conductivity (W/(m K))	Density (kg/m^3)	Heat capacity (J/(kg K))
Epoxy resin	1e−15	0.92 − 0.21e−2 T	1037.90 − 0.27 T	1650
Aluminum	1/(6.62e−17T^3 − 8.19e−14T^2 + 1.45e−10 T − 1.04e−8)	464.14 − 2.84 T + 1.25e−2T^2 − 2.34e−5T^3 + 1.57e−8T^4	2751.78 − 0.18 T + 4.66e−5T^2 − 1.52e−7T^3 + 6.83e−11T^4	595.66 + 1.51 T − 0.21e−2T^2 + 1.30e−6T^3

The loss obtained from solving the electromagnetic field is added as a heat source to the solid heat transfer equation to achieve the coupling of the electromagnetic and thermal. In Eq. (8), Newton's law of cooling and Stefan Boltzmann's law are used to describe the convection and radiation heat transfer between the bushing surface and the air.

The calculation considers the relationship between the electromagnetic properties of the material and temperature to achieve bidirectional coupling of the heat and electromagnetic field. The parameters used of the material of the bushing in the calculation are shown in Table 1.

3 Simulation Results and Analysis

3.1 Under Normal Conditions

The internal electric field distribution of the simulated bushing is shown in Fig. 3a and b. It can be seen that there is a high field strength area in the center of the installation flange where the bushing through the cabinet. As the calculation result, the maximum field strength value inside the bushing is 809 kV/m, which appears on the inner surface of the bushing crossing the wall.

Figure 3c and d respectively show the radial field strength curves along the axis parallel to the busbar and perpendicular to the busbar. It can be seen that in the direction of the busbar, the internal electric field gradually decreases from the end of the cabinet to the outer end of the bushing, with a maximum value of 125 kV/m, appearing at the wall penetration of the cabinet. In the direction perpendicular to the busbar, there are double peaks in the field strength on the inner surface of the bushing, which appear at the upper and lower flush ends of the bushing and the conductive busbar. The peak field strength is maintained at 111 kV/m, and the lowest field strength value is 763 V/m, appearing at the center of the upper surface of the bushing.

The steady-state temperature distribution of the bushing under normal condition is shown in Fig. 4. It can be seen that the overall temperature of the bushing decreases from the middle section to both sides. The highest temperature value in the air domain

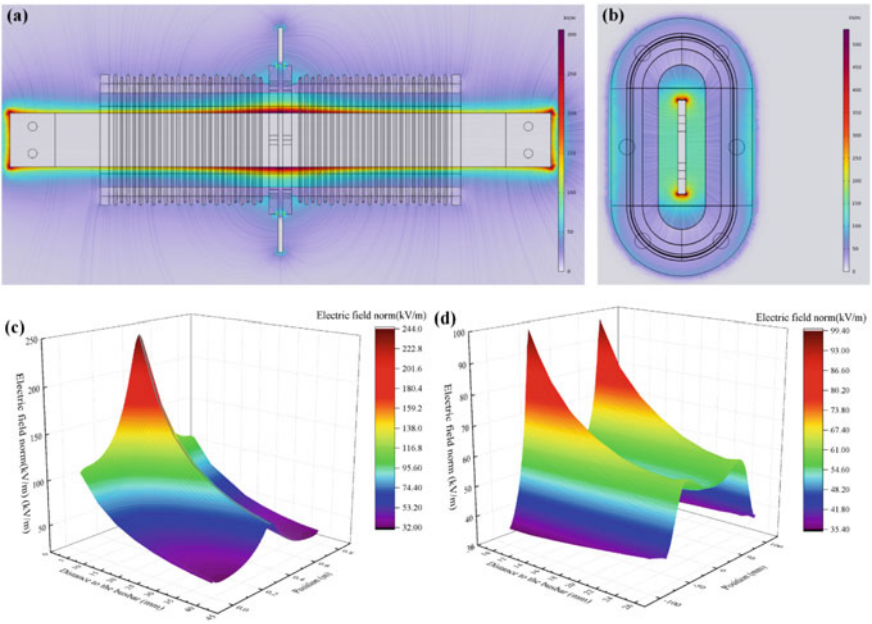

Fig. 3 **a** Electric field distribution on the axial section of the bushing. **b** Electric field distribution on the radial section of the bushing. **c** Axial electric field distribution. **d** Radial electric field distribution

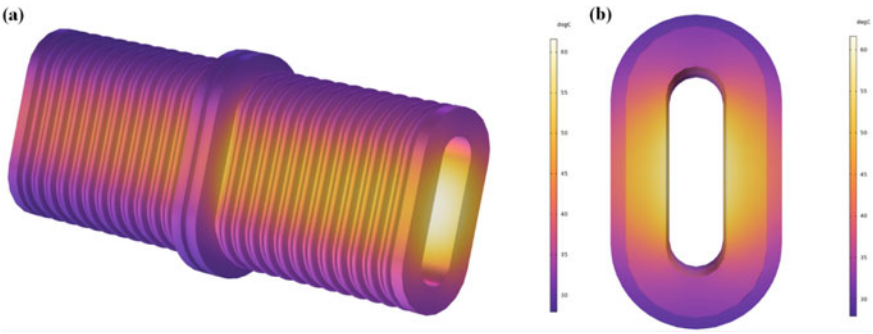

Fig. 4 Temperature distribution of the bushing. **a** Axial section. **b** Radial section

is 54.4 °C, which appears at the center of the bushing near the busbar. The temperature rise of the bushing body is mainly reflected on the inner surfaces on the left and right sides, as well as the parts on the inner side which are flush with the busbar. The maximum temperature value on the surface of the bushing is 56.6 °C, which occurs on the side surface of the middle section where the bushing does not pass through the cabinet. The minimum value is 27.3 °C, located at the outer end of the bushing.

3.2 Under Defect Conditions

To simulate the operation of the bushing during the short-circuit fault, the electromagnetic and thermal field were calculated again on the bushing with added insulation defects under the condition of three-phase short-circuit. In defect conditions, the short-circuit current of the busbar is 19.6 kA, with a duration of 1.69 s. The calculated electric field distribution of the bushing at peak time is shown in Fig. 5.

It can be seen that when there is an air gap inside the bushing, there is distortion of the electric field, and two high field strength regions appear at the air gaps 1 and 2, which are much greater than the surrounding area. The maximum value can reach 427 kV/m, which is far greater than the breakdown field strength of air. At this gap distance, it will lead to breakdown discharge within the air gap, which in turn will lead to the degradation of the epoxy resin. When the internal deterioration of the bushing reaches a certain level, it will cause a wide range of internal breakdown and discharge, ultimately leading to a short circuit explosion accident.

Figure 6 compares the steady-state temperature distribution of the bushing under normal condition with that when the busbar passes the first short-circuit current and triggers the warning. It can be seen that due to the presence of abnormal short-circuit current and air gap discharge, the temperature of the epoxy bushing has significantly increased, with a maximum value of 114.6 °C. The minimum temperature of the entire bushing is 55.6 °C, which still appears at the outer port.

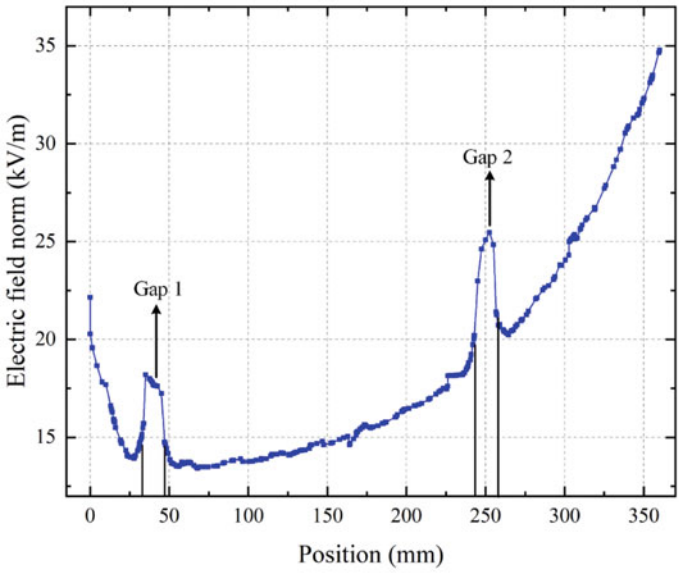

Fig. 5 Electric field distribution inside the bushing

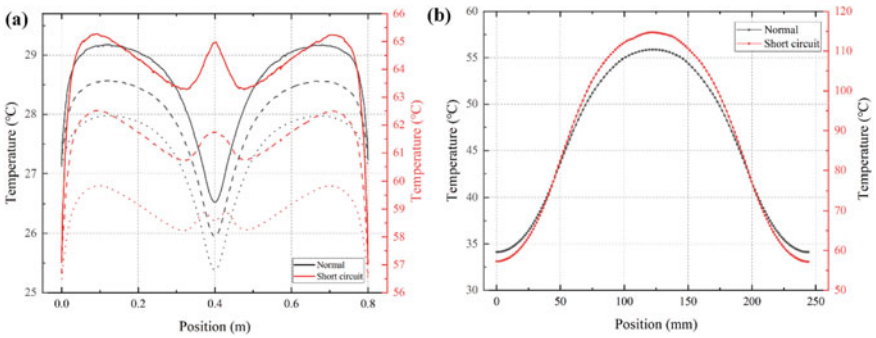

Fig. 6 Temperature distribution of the bushing **a** Axial section. **b** Radial section

3.3 Discharge Analysis

In order to further verify the effect of air gap on the insulation failure of the bushing, the Electrical breakdown detection interface in the COMSOL plasma module is used for the discharge analysis of the defective bushing. It is difficult to establish a fully self-consistent discharge plasma model due to the complex structure of the bushing and the cabinet. Therefore, this paper uses a method by integrating the Townsend growth coefficient along the electric field line to estimates whether the Electrical breakdown will occur in the air gap without solving the complete plasma model [11].

The breakdown condition for self-sustaining discharge in gas is:

$$\gamma_i \left(\exp\left(\int_0^D N\alpha ds \right) - 1 \right) = 1 \tag{9}$$

where γ_i is the secondary emission coefficient, N is the Number density, α is the converted Townsend growth/Attenuation coefficient, S is the arc length along the ion particle trajectory, and D is the distance from the source boundary to any target boundary. By using this formula, we can divide the discharge in the test gas into three situations:

1. No discharge:

$$\int_0^D N\alpha ds < \ln\left(1 + \frac{1}{\gamma_i}\right) \tag{10}$$

2. Continuous discharge:

$$\int_0^D N\alpha ds > \ln\left(1 + \frac{1}{\gamma_i}\right) \tag{11}$$

3. Streamer discharge:

$$\int_0^D N\alpha ds > 17.7 + \ln(d/1[\text{cm}]) \tag{12}$$

In the calculation, information from all three states is embedded in the converted Townsend growth coefficient α, it is a strong function of the reduced electric field:

$$\alpha = \alpha\left(\frac{E}{N}\right) \tag{13}$$

where E is the electric field parallel to the streamline, the integral is calculated by solving the Ordinary differential equation along the test particle trajectory:

$$\frac{d\alpha_D}{ds} = \alpha\left(\frac{N}{N_{stp}}\right) \tag{14}$$

where N_{stp} is the Number density at standard temperature and pressure. The Townsend growth coefficient of dry air in the calculation was interpolated using the growth coefficient relative to the reduced electric field [12].

Figure 7a shows the simulated Electrical breakdown indicator. In the breakdown indicator, 0 represents no breakdown and there's no discharge will occur, 1 represents Townsend discharge (current limiting), and 2 represents the streamer with infinite current flow. Due to the different distribution of air gap positions, their breakdown situations vary. In the four gaps of ABCD, there is no breakdown and discharge in gap D which is far from the side surface. While Townsend discharge will occur in gaps B and C which near the center of the side surface, with a low possibility of producing streamers at the center of the gap. There is already a great possibility of large-scale streamer discharge occurring in gap A which is closest to the cabinet.

Figure 7b shows the calculation results of the integral Townsend growth coefficient, which forms a streamer when its value is higher than 18.3. The integral growth coefficient in gap BCD is basically lower than the streamer's threshold, where the value in D is much smaller than that in BC. This result indicates that there is a greater

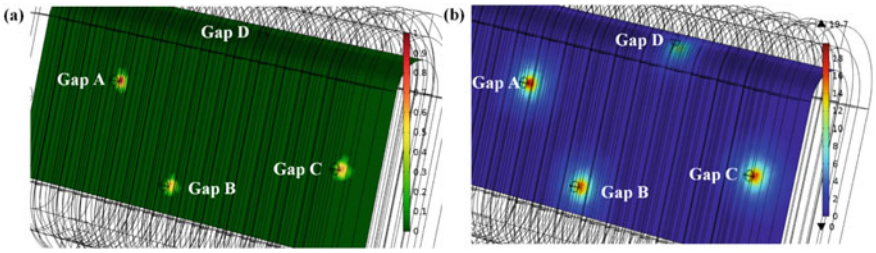

Fig. 7 **a** Breakdown indicator. **b** Integral Townsend growth coefficient

likelihood of more severe discharge when the air gap appears on the side surface of the bushing or near the side of cabinet.

4 Conclusions

1. The insulation structure of the bushing is damaged when there are air gaps inside it, and the internal electric field distortion and abnormal temperature rise can lead to the deterioration and denaturation of the epoxy resin.
2. There is a greater likelihood of more severe discharge occurring when the air gap appears on the side surface of the bushing or near the cabinet side.
3. Partial discharge live detection should be carried out during the operation and maintenance of the cabinet bushing to detect the discharge in the air gaps as early as possible and prevent further faults from occurring.

References

1. Zhixiang DENG, Chen KANG, Huayun WANG et al (2019) Partial discharge detection and structure optimization of bushing for 10 kV switchgear. Insulators Surge Arresters 2:226–230 (in Chinese)
2. Zhifeng LUO, Xian CAO, Boyong WANG et al (2021) Climbing field strength calculation and structure optimization of 10 kV switchgear casing inner wall. J Nanchang Univ (Eng Tech) 43(2):191–196 (in Chinese)
3. Yongyong J, Jinggang Y, Shan G et al (2017) Simulation of internal electric field of high-voltage metal-enclosed switchgear and influencing factors. High Voltage Apparatus 53(6):154–160 (in Chinese)
4. Haiyan W, Zhihao Z, Xiang F et al (2019) Electric field optimization and structure design of wall bushing in 40.5 kV air-insulated switchgear. High Voltage Apparatus, 55(1):59–63 (in Chinese)
5. Xiaolei ZHAO, Jun HU, Zhikang YUAN et al (2021) Design of adaptive bushing based on field grading materials. High Voltage 6(4):625–636
6. Haowei YAO, Kefeng LV, Zhen LOU et al (2023) Simulation study on oil pressure problems caused by internal faults in oil-immersed transformers. Process Saf Environ Prot 175:190–198

7. Shiling Z, Zongren P (2020) Application of finite element method in three-dimensional electric field simulation of UHVDC wall bushing. High Voltage Eng 46(03): 782–789 (in Chinese)
8. Shiling Z, Zongren P, Peng L et al (2015) Design and dielectric characteristics of the ±1100 kV UHVDC wall bushing in China. IEEE Trans Dielectr Electr Insul 22(1):409–419
9. Dexin N, Hailong Z, Zhong C et al (2013) Optimization design of grading ring and electrical field analysis of 800 kV UHVDC wall bushing. IEEE Trans Dielectrics and Electr Insul 20(4) 1361–1368
10. Monga S, Gorur RS, Hansen P, Massey W (2006) Design optimization of high voltage bushing using electric field computations. IEEE Trans Dielectr Electr Insul 13:1217–1224
11. Larry KW, Jorgenson RE, Nicolaysen SD (2003) Ionization coefficient approach to modeling breakdown in nonuniform geometries. Sandia Report
12. Dutton J (1975) A survey of electron swarm data. J Phys Chem Ref Data 4(3):577–856